Resonance measurements of d-f-g-h splittings in highly excited states of sodium*

T. F. Gallagher, R. M. Hill, and S. A. Edelstein
Molecular Physics Center, Stanford Research Institute, Menlo Park, California 94025
(Received 12 April 1976)

Using two- and three-photon resonance techniques, we have observed d-g and d-h transitions in the $n = 13$ to 17 states of sodium. The results yield accurate values for the quantum defects of the d, f, g, and h states as well as the fine-structure splitting of the levels. Although the d ($l = 2$) fine structure is inverted, for $l > 2$ the fine structures are observed to be hydrogenic.

I. INTRODUCTION

The highly excited or Rydberg states of sodium are essentially hydrogenic in character, the small differences arising from the penetration and polarization of the ionic core by the valence electron.[1] These interactions lead to such nonhydrogenic behavior as the nondegeneracy of the l states of the same n (usually characterized by a quantum defect δ) and the inversion of the d-state fine-structure levels. Accurate measurements of the Δl energy separations and the fine-structure intervals should allow a quantitative understanding of the interactions of the valence electron and the ionic core, enabling one to accurately predict the locations of the levels.

The advent of the tunable dye laser has made possible a variety of methods for the efficient production and detection of single n, l Rydberg states.[2-4] Sodium atoms have been excited to states of high enough n that the frequency separation of the d state from the higher l states falls in the range covered by standard microwave sources. Taking advantage of this, we have used a laser-excitation optical detection scheme to make microwave–radio-frequency (rf) resonance measurements of the d-f-g-h Δl energy separations and fine-structure intervals in a series of highly excited n levels of sodium. The one-photon d-f measurements have been reported previously[5] and are similar to the measurements performed by MacAdam and Wing on helium.[6] In the d-g measurements reported here, two microwave photons of the same frequency were used to drive the two-photon d-g transitions.

Although two-photon spectroscopy is quite new in optical spectroscopy, it has long been known in molecular-beam rf spectroscopy, being first observed by Hughes and Grabner[7] in 1950. The three-photon d-h measurements, which were done with one microwave and two rf photons of the same frequency, are a logical extension of the two-photon d-g measurements.

II. EXPERIMENTAL METHOD

The basic technique which we have used to measure the d-g separations is shown in Fig. 1. Two dye lasers are used to sequentially excite the sodium atoms from $3s$ to $3p$ and from $3p$ to nd. The microwave field at resonance causes the atoms to undergo transitions to the g state, from which about one-third of the atoms decay to the $4f$ state then to the $3d$ state. Using an infrared (ir) filter and a photomultiplier, we detect the $3d$-$3p$ fluorescence at 8197 Å. As the microwave frequency is swept through the two-photon d-g resonance, a sharp increase in the ir fluorescence is observed, as shown in Fig. 2. There is a small amount of background ir fluorescence due to cascades and collisional mixing of the l states originating from the excited high-d state.[8]

The d-h measurements were essentially the same as the d-g measurements in that we detected an increase in the $3d$-$3p$ fluorescence as we swept the microwave frequency through the d-h resonance. The difference was that we used a rf field as well as a microwave field. The frequencies were chosen so that we used two rf photons and one microwave photon, as shown by the level diagram of Fig. 3. We fixed the rf frequency and swept the microwave frequency through the three-photon d-h resonance. Although the increase in the fluorescence at the d-h resonance is not as strong as for the d-f and d-g resonances, it is still observable, as shown in Fig. 4.

Since most of the apparatus is described elsewhere,[9] we give only a brief description here. The major components of the apparatus are shown in the block diagram of Fig. 5. The sodium is contained in a cylindrical pyrex cell 2.5 cm in diameter and 10 cm long which is heated to 175 °C, providing a sodium pressure of 5×10^{-5} Torr. A N_2 laser pumps two dye lasers. The two dye-laser beams, which intersect at a slight angle at the center of the cell, pass through the cell nearly on its axis. The microwaves are introduced from

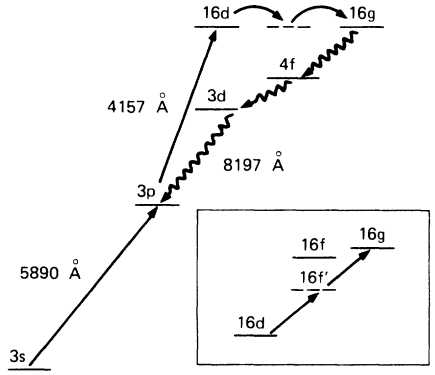

FIG. 1. Relevant energy levels for the observation of the two-photon d-g resonance in the $n=16$ state of sodium. The straight arrows are the two laser pumping steps; the wavy arrows down indicate the most probable fluorescent decay of the $16g$ state. We observe the $3d$-$3p$ fluorescence at 8197 Å. The inset shows the location of the d, f, and g states, as well as the virtual state f' through which the two-photon process proceeds.

the direction perpendicular to the cell axis by simply ending a waveguide (using a horn in the high-frequency bands) as close to the side of the cell as possible.

The rf field was introduced by putting a helical loop, of pitch equal to its diameter, around the cell. The loop consisted of six fine copper wires, effectively making a strap 4 mm wide. This configuration was chosen to provide an electric field of reasonable strength at the center of the cell and to form a transmission line of roughly 50 Ω impedance. It was important that the impedance be roughly 50 Ω, so that impedance mismatches would not cause such serious reflections as to prevent the rf field from getting onto the loop.

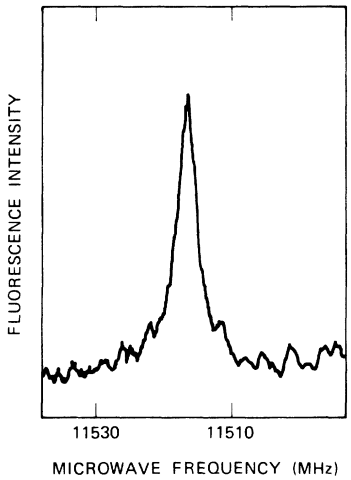

FIG. 2. Two-photon $16d_{3/2}$-$16g_{7/2}$ resonance on a sweep of increasing frequency.

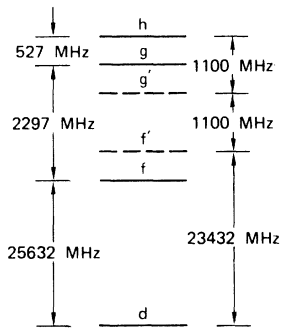

FIG. 3. Energy-level diagram for showing the real and virtual levels involved in the three-photon d-h resonance for $n=15$. On the left-hand side the intervals between the real states are given, and on the right-hand side are shown the intervals between the virtual states showing the approximate frequencies used.

The ir fluorescence signal was detected by a photomultiplier and integrated by a PAR 162 boxcar integrator with a 3-μsec gate. The boxcar output was recorded on one channel of a strip chart recorder. On the second channel, we recorded the microwave power transmitted to a crystal detector through the Hewlett-Packard (HP) 532 wavemeter appropriate for the frequency range. This arrangement produced a frequency marker at the wavemeter setting. The frequency of the microwave source was swept slowly through the resonance frequency, and the wavemeter was set twice on each scan, once above and once below the resonance frequency, to produce frequency markers above and below the resonance. Sweeping up and down in frequency was necessary to cancel apparent offsets in the resonance frequency produced by the time constant of the boxcar averager.

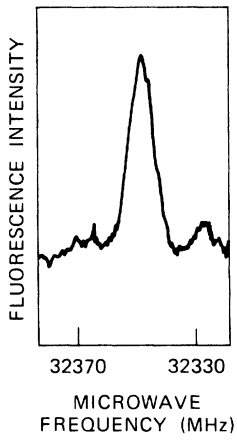

FIG. 4. Three-photon $14d_{3/2}$-$14h_{9/2}$ resonance on a sweep of increasing frequency. The rf frequency was 1288.9 MHz.

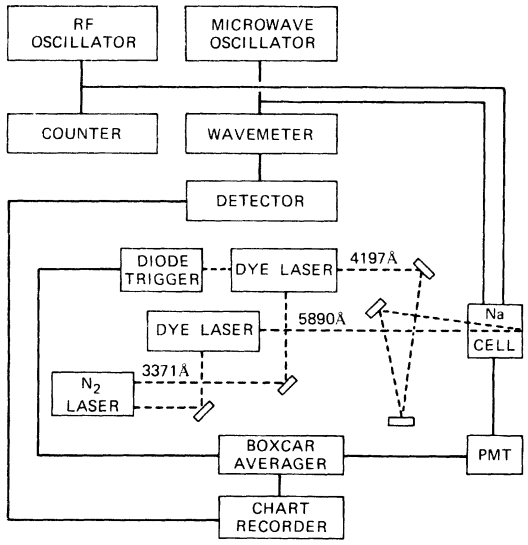

FIG. 5. Block diagram of the apparatus, with the lasers tuned to populate the $13d_{5/2}$ level.

For a rf source, we used a General Radio 1218A oscillator and monitored its frequency with a HP 5245 counter. We used various microwave sources for the frequencies below 18 GHz and a HP 8690 sweeper for frequencies above 18 GHz. The microwave frequencies were measured with the wavemeters, which were in turn calibrated using a HP 5340A microwave counter. The error in setting the wavemeter was ±0.6 MHz at 40 GHz and proportionally less at lower frequencies.

III. EXPERIMENTAL CONSIDERATIONS

The success of the multiphoton resonance experiments depends critically upon several factors. First, we must have enough microwave and rf power to drive the multiphoton transitions. At the same time, we have to be able to account for the level shifts produced by the strong fields required to drive the transitions. Finally, there must be enough signal to observe the resonances.

First, let us consider the power requirements. The lifetimes of the Rydberg states near $n=15$ are short, ~3 μsec, and we must induce a transition in that short time. Consequently, one might expect that high rf or microwave power would be necessary to drive the multiphoton transitions.

It is necessary only that power be high enough so that the rf-microwave transitions are induced at a rate exceeding the d-state radiative decay rate. To calculate the transition rates, we need the relevant dipole matrix elements. In atomic units (ea_0) the hydrogenic $\Delta m=0$ matrix elements $\langle nl|\mu|nl+1\rangle$ are given by Bethe and Salpeter[10] as

$$\langle nl|\mu|nl+1\rangle=\left(\frac{(l+1)^2-m^2}{(2l+3)(2l+1)}\right)^{1/2}\times\frac{3n}{2}[n^2-(l+1)^2]^{1/2}. \tag{1}$$

Consider the specific example of the $n=15$, $m=0$ level. The relevant matrix elements then, in units of ea_0 and D, are

$$\begin{aligned}&\langle d|\mu|f\rangle=165ea_0=412\text{ D},\\&\langle f|\mu|g\rangle=160ea_0=400\text{ D},\\&\langle g|\mu|h\rangle=155ea_0=388\text{ D}.\end{aligned} \tag{2}$$

The transition rates (in MHz) for the three types of transitions are then given by

$$k_{d\text{-}f}\cong\tfrac{1}{2}\langle d|\mu|f\rangle E_{\rm mw}, \tag{3a}$$

$$k_{d\text{-}g}\cong\frac{1}{4}\frac{\langle d|\mu|f\rangle\langle f|\mu|g\rangle}{|W_f-W_{f'}|}E_{\rm mw}^2, \tag{3b}$$

$$k_{d\text{-}h}\cong\frac{1}{8}\frac{\langle d|\mu|f\rangle\langle f|\mu|g\rangle\langle g|\mu|h\rangle}{|W_f-W_{f'}||W_g-W_{g'}|}E_{\rm mw}E_{\rm rf}^2, \tag{3c}$$

where the factors $\frac{1}{2}$, $\frac{1}{4}$, and $\frac{1}{8}$ reflect the conversion factor 1 D × 1 V/cm = $\frac{1}{2}$ MHz, the microwave and rf fields $E_{\rm mw}$ and $E_{\rm rf}$ are given in V/cm, and $W_l-W_{l'}$ is the frequency separation of the real and virtual intermediate states in MHz. The peak field strengths and power required to produce a 1-MHz transition rate for the $n=15$ transitions are listed in Table I. For the d-g case $W_f-W_{f'}$ = 11 700 MHz. For the d-h case $W_g-W_{g'}=|W_f-W_{f'}|$ = 600 MHz. These power requirements are modest enough so that these experiments may be carried out with readily available microwave and rf sources. In practice the power levels listed in Table I are in good agreement with our observations.

The electric field strengths necessary to induce

TABLE I. rf powers required to produce a transition rate of 1 MHz in the $n=15$ d-l transitions.

Transition	Number of photons	rf frequency (GHz)	Peak electric field (V/cm)	rf power required (mW)
d-f	1	25.6	4.8×10^{-3}	1×10^{-3}
d-g	2	13.9	0.64	5
d-h	2	1.1	0.48	40
d-h	1	26.3	0.48	5

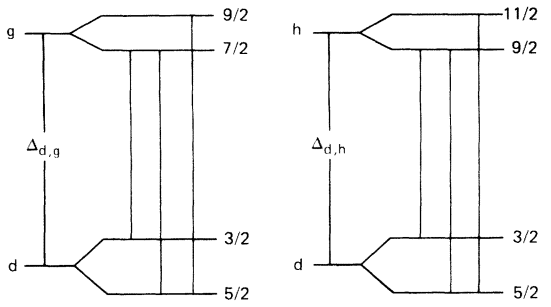

FIG. 6. Energy-level diagrams showing $\Delta_{d,g}$ and $\Delta_{g,h}$, the energy separations unperturbed by fine structure, the fine-structure splittings, and the allowed transitions.

multiphoton transitions frequently produce frequency shifts. This phenomenon is most generally known as the ac Stark effect. Current research into ac Stark shifts is typified by the investigations of light shifts in two-photon optical spectroscopy by Liao and Bjorkholm.[11] Historically, rf Stark shifts have been observed in molecular-beam rf spectroscopy by Marple and Trishka[12] and in microwave spectroscopy by Autler and Townes,[13] who have developed a comprehensive theory of rf Stark shifts. For our purposes the important features to note are that the frequency shifts are proportional to the square of the rf electric field and thus to the rf power, and that the microwave and rf Stark shifts may be determined independently. The practical consequence of this is that we may vary the rf and microwave power separately and extrapolate the measured frequencies to zero power.

Since we observe the d-l resonances (here l may be f, g, or h) by detecting fluorescence emitted by atoms which radiatively decay from the higher l state, the radiative lifetimes of the l states affect both the observed linewidths and the strength of the signals. The effect on the signal is best illustrated by considering a simple picture. Assume that the microwave field is causing the atoms to undergo the d-l transition at a rate k_T, which is faster than the d-state radiative decay rate $1/\tau_d$. Then the atoms decay at the average of the d and l state radiative rates $\frac{1}{2}(1/\tau_d + 1/\tau_l)$. The resonance signal is proportional to the fraction of the atoms which radiatively decays from the higher l state. This fraction S is proportional to the radiative decay rate of the l state and is given by

$$S = \frac{1/\tau_l}{1/\tau_d + 1/\tau_l} = \frac{1}{1 + \tau_l/\tau_d}. \tag{4}$$

Thus the longer radiative lifetimes of the higher l states lead to lower signals. In practice we found that the d-h resonance signal was typically equal to half the background fluorescence, so that to see a transition to an i state would probably require a more refined technique.

TABLE II. Extrapolated d-g resonance frequencies and energy separations. The number in parentheses is the uncertainty in the final digit(s).

Transition	Frequency (MHz)	d-g separation (MHz)
$13d_{3/2}$-$13g_{7/2}$	21 354.4(6)	42 708.8(12)
$13d_{5/2}$-$13g_{9/2}$	21 380.0(6)	42 760.0(12)
$14d_{3/2}$-$14g_{7/2}$	17 132.1(6)	34 264.2(12)
$14d_{5/2}$-$14g_{9/2}$	17 149.9(9)	34 299.8(18)
$15d_{3/2}$-$15g_{7/2}$	13 955.2(9)	27 910.4(18)
$15d_{5/2}$-$15g_{9/2}$	13 969.1(4)	27 938.2(8)
$16d_{3/2}$-$16g_{7/2}$	11 515.2(4)	23 030.4(8)
$16d_{5/2}$-$16g_{9/2}$	11 528.5(4)	23 057.0(8)
$17d_{3/2}$-$17g_{7/2}$	9611.2(3)	19 222.4(6)
$17d_{5/2}$-$17g_{9/2}$	9621.1(3)	19 242.2(6)

IV. OBSERVATIONS

One d-g resonance was observed for each of the $nd_{3/2}$ and $nd_{5/2}$ states at several microwave power levels. However, as can be seen from Fig. 6, a total of three transitions is allowed, the $\Delta J = 2$ $d_{3/2} \rightarrow g_{7/2}$, the $\Delta J = 1$ $d_{5/2} \rightarrow g_{7/2}$, and the $\Delta J = 2$ $d_{5/2} \rightarrow g_{9/2}$ transitions. To decide which of the two transitions originating from the $nd_{5/2}$ states we observe, we must consider the relative transition probabilities. The $\Delta J = 2$ transition rate is proportional to the product of two $\Delta J = 1$ electric dipole transition matrix elements. The $\Delta J = 1$ transition rate is a product of one $\Delta J = 1$ matrix element and one $\Delta J = 0$ matrix element. The $\Delta J = 0$ matrix elements are calculated to be a factor of 10 smaller

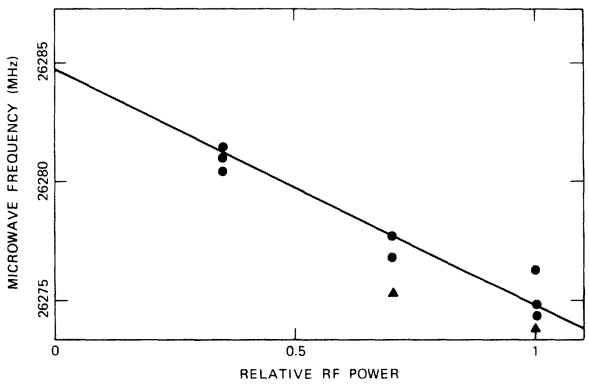

FIG. 7. Extrapolation of the $15d_{3/2}$-$15h_{9/2}$ three-photon resonance to zero rf power. Two relative microwave powers are indicated, 1.0 (▲) and 0.1 (●). At the relative microwave power of 1.0, the microwave field was ~1 V/cm.

TABLE III. Extrapolated d-h separations.

Transition	rf frequency (MHz)	Microwave frequency (GHz)	d-h separation (MHz)
$13d_{3/2}$-$13h_{9/2}$	1890	39.74	43 516(4)
$13d_{5/2}$-$13h_{11/2}$	1890	39.79	43 565(4)
$14d_{3/2}$-$14h_{9/2}$	1280	32.36	34 922(4)
$14d_{5/2}$-$14h_{11/2}$	1280	32.40	34 958(4)
$15d_{3/2}$-$15h_{9/2}$	1080	26.29	28 446(3)
$15d_{5/2}$-$15h_{11/2}$	1080	26.32	28 476(3)
$16d_{5/2}$-$16h_{11/2}$	960	21.57	23 490(15)

than the $\Delta J = 1$ matrix elements. Consequently, when the microwave power is adjusted to produce the narrowest-linewidth maximum-amplitude signal for the $\Delta J = 2$ resonance, the transition rate, and hence the signal, for the $\Delta J = 1$ resonance is a factor of 10 lower. The frequency separation between the two resonances is half the g-state fine-structure interval, which is roughly equal to the half-width of the observed resonances. Unfortunately, the quality of the data does not permit us to deconvolute the observed resonance peak into one large- and one small-amplitude peak. Thus we have assigned the observed resonance as the stronger $\Delta J = 2$ resonance. This assignment is supported by the observation that at the same microwave power the $\Delta J = 2$ $d_{3/2}$-$g_{7/2}$ resonance had the same linewidth. The values listed in Table II are the two-photon frequencies extrapolated to zero microwave power, assuming a frequency shift linear in the microwave power. Depending on the microwave power, the measured frequencies were 0.5–2 MHz higher than the values in Table II, so the shifts were only slightly larger than the scatter of the data.

To verify that we were observing d-h three-photon transitions, for $n = 14$ and 15 we increased the rf frequency over a range of 50 MHz and noted that the microwave frequency at which the resonance occurred decreased twice as fast. This indicated that the process required two rf photons for each microwave photon and was thus the three-photon d-h transition.

Although the three d-h transitions shown in Fig. 6 should be observable, we were able to observe only one d-h resonance for each of the $nd_{3/2}$ and $nd_{5/2}$ states which we assigned as $\Delta J = 3$ transitions, for the same reason that we assigned the two-photon d-g resonances as $\Delta J = 2$ transitions. To find the true d-h separation, we attempted to make both rf and microwave power shift measurements. This proved to be difficult, mainly because the signal was marginal at the highest powers. Nonetheless, we were at least moderately successful in doing this for $n = 15$. In Fig. 7 we show the power dependence of an $n = 15$ resonance frequency. As shown in Fig. 7 the rf power shifted the d-h frequency as much as 8 MHz below the zero power frequency, and the microwave power shifts were ~2 MHz. Both results were in accord with our estimates based on the theory of Autler and Townes.[13] The extrapolated d-h separations, as well as the approximate rf and microwave frequencies used, are given in Table III.

There is one other effect which shifts the apparent location of the three-photon d-h resonance. The observed microwave frequencies are in all cases within 1 GHz of the power-broadened one-photon d-f resonance, so that the d-h peak sits on the shoulder of the much stronger d-f resonance. We have calculated that the apparent shift due to this is ~0.2 MHz, which is negligible.

The d-g linewidths of 3–4 MHz and the d-h linewidths of 10–15 MHz are noticeably larger than the d-f linewidths of 2–3 MHz. We attributed this mostly to the variations in the rf Stark shifts produced by the spatial inhomogeneities of the rf and microwave fields. We estimate that the squares of both the rf and microwave fields vary by a factor of 2 over the active region of the cell (that which is excited by the laser and observed

TABLE IV. Theoretical S_{lt} and experimental S_{lx} fine-structure splittings of the f, g, and h sublevels of sodium.

n \ l	f		g		h	
	S_{ft} [a]	S_{fx} [b]	S_{gt} [a]	S_{gx}	S_{ht} [a]	S_{hx}
13	6.65	6.4(20)	3.32	7.2(36)	2.21	5(7)
14	5.32	5.0(8)	3.19	0.7(35)	2.13	1(7)
15	4.33	3.5(16)	2.60	1.7(36)	1.73	4(7)
16	3.56	2.9(11)	2.13	1.6(25)		
17	2.97	2.1(10)	1.78	0.5(32)		

[a] Calculated for hydrogen. See Ref. 10, p. 61.
[b] See Ref. 5.

by the photomultiplier). This implies that the broadening should be roughly the same size as the shift, in qualitative agreement with our observations.

V. FINE-STRUCTURE RESULTS

From the data of Sec. IV and previous work,[5] we can readily determine the fine-structure splittings S_l of the f, g, and h levels, which are tabulated in Table IV. We have also listed for comparison the theoretical fine structure of hydrogen for these levels. It is important to note that although the sodium d fine-structure levels are inverted, the f fine-structure levels are not, and furthermore are in excellent agreement with the theoretical hydrogen fine-structure splittings. Within the precision of the data, the measured g and h fine-structure splittings are in agreement with theory, but the data are not sufficiently accurate to warrant much further comment. Since the f fine structure is hydrogenic, it seems reasonable to assume that the higher l states are also.

VI. QUANTUM DEFECTS

Historically, the energy levels of sodium have been expressed as

$$W_{nl} = -\mathcal{R}^*/(n-\delta_l)^2, \tag{5}$$

where W_{nl} is the energy of the nl state unperturbed by fine structure, $\mathcal{R}^*$ is the Rydberg constant corrected for the finite mass of the sodium nucleus, 109 734.7 cm^{-1}, n is the principal quantum number, and δ_l is the phenomenological quantum defect of the states of angular momentum l. The energy difference (unperturbed by fine structure) between two l states $\Delta_{l,l'}$, which we measure, is related to the quantum defects by

$$\Delta_{l,l'} = W_{l'} - W_l = \mathcal{R}^*/(n-\delta_l)^2 - \mathcal{R}^*/(n-\delta_{l'})^2. \tag{6}$$

Using the binomial theorem, this may be expressed as

$$\Delta_{l,l'} = (\mathcal{R}^*/n^3)[2(\delta_l - \delta_{l'}) + 3(\delta_l^2 - \delta_l^2)/n + \cdots]. \tag{7}$$

TABLE V. Quantum defects of the d, f, g, and h states of Na.

n	$10^2\delta_d$	$10^3\delta_f$	$10^4\delta_g$	$10^4\delta_h$
13	1.4653(5)	1.585(4)	4.155(30)	1.466(15)[a]
14	1.4688(5)	1.592(4)	4.219(33)	1.479(15)[a]
15	1.4719(6)	1.601(5)	4.242(35)	1.489(15)[a]
16	1.4751(6)	1.611(5)	4.329(43)[a]	
17	1.4759(7)	1.603(5)	4.252(43)[a]	

[a] Calculated by Freeman and Kleppner, Ref. 14.

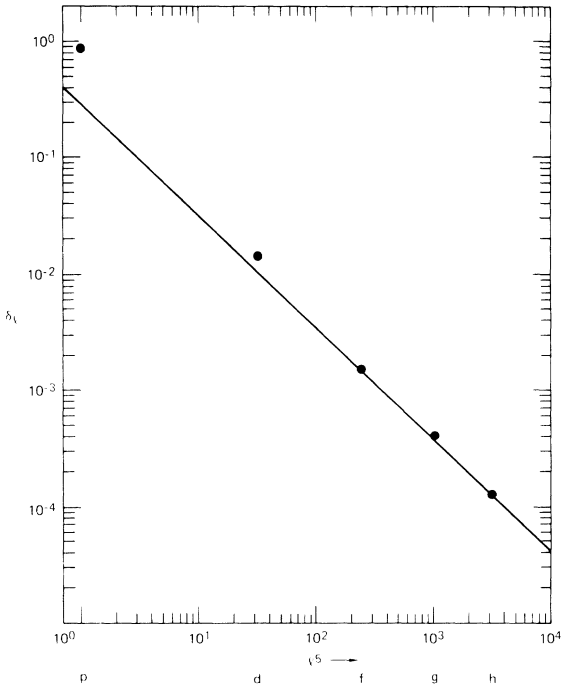

FIG. 8. log-log plot of the quantum defect δ_l vs l^5. The line through the f, g, and h quantum defects reflects the l^{-5} character of core polarization. The additional effect of core penetration on the p and d levels is quite apparent.

The second term is important only when dealing with the d and f quantum defects, in which case Eq. (7) may be solved by iteration. The $\Delta_{l,l'}$ splittings can be derived from the data of Sec. IV by simply taking fine structures into account. Then, by inverting Eq. (7), we are able to calculate the differences in the quantum defects. Using the data presented here and in Ref. 5, Freeman and Kleppner[14] have calculated the actual quantum defects for the highest l state which we observed for each value of n. Combining their calculated values for the quantum defects of the high-l states with the differences we can calculate using Eq. (7), we are able to derive with high accuracy the quantum defects presented in Table V. It is interesting to note that quantum defects increase regularly, although slowly, with n. Perhaps more interesting, though, is the l dependence of δ_l. If the δ_l values of Table V, together with the quantum defect δ_p of the p states, 0.85, are plotted vs l^5 on a log-log graph, we have the result shown in Fig. 8.

The graph shows clearly that only core polarization, which varies as l^{-5} (Ref. 14), is responsible for the quantum defects of the $l>2$ states. Core penetration is important only for the lower l states. It is interesting to note that is the d level (the highest-l state for which core penetration

is important) which exhibits the inverted fine structure, strongly suggesting the relation between core penetration and fine-structure inversion.

We believe that the experiments described here are only the beginning of a powerful new technique in atomic spectroscopy. The techniques can be refined in countless ways to achieve greater precision and sensitivity. It appears that this technique will be quite useful in investigating many aspects of the interactions of valence electrons with their ionic cores.

ACKNOWLEDGMENTS

We would like to acknowledge helpful discussions with R. R. Freeman, D. Kleppner, and K. B. MacAdam. We are particularly grateful to J. Watjen, U. Gysel, and A. Karp for their help and encouragement in coping with our microwave problems, as well as for loaning us microwave equipment. We are also indebted to S. Tetenbaum, E. Fernandez, and G. Tomlin for the generous loans of microwave equipment.

---

*Work supported by the Air Force Office of Scientific Research under Contract No. F44620-74-C-0069.

[1]E. U. Condon and G. H. Shortley, *The Theory of Atomic Spectra* (Cambridge U. P., Cambridge, 1964).

[2]C. Fabre, M. Gross, and S. Haroche, Opt. Commun. 13, 393 (1975).

[3]T. W. Ducas, M. G. Littman, R. R. Freeman, and D. Kleppner, Phys. Rev. Lett. 35, 366 (1975).

[4]R. F. Stebbings, C. J. Latimer, W. P. West, F. B. Dunning, and T. B. Cook, Phys. Rev. A 12, 1453 (1975).

[5]T. F. Gallagher, R. M. Hill, and S. A. Edelstein, Phys. Rev. A 13, 1448 (1976).

[6]K. B. MacAdam and W. H. Wing, Phys. Rev. A 12, 1464 (1975).

[7]V. Hughes and L. Grabner, Phys. Rev. 79, 829 (1950).

[8]T. F. Gallagher, S. A. Edelstein, and R. M. Hill, Phys. Rev. Lett. 35, 644 (1975).

[9]T. F. Gallagher, S. A. Edelstein, and R. M. Hill, Phys. Rev. A 11, 1504 (1975).

[10]H. A. Bethe and E. E. Salpeter, *Quantum Mechanics of One and Two Electron Atoms* (Academic, New York, 1957), pp. 17 and 253.

[11]P. F. Liao and J. E. Bjorkholm, Phys. Rev. Lett. 34, 1 (1975).

[12]D. T. F. Marple and J. W. Trishka, Phys. Rev. 103, 597 (1956).

[13]S. H. Autler and C. H. Townes, Phys. Rev. 100, 703 (1955).

[14]R. R. Freeman and D. Kleppner (unpublished).